Experimental evaluation of the intrinsic noise in the Couette-Taylor system with an axial flow

Avraham Tsameret, Galia Goldner, and Victor Steinberg
Department of Nuclear Physics, The Weizmann Institute of Science, Rehovot 76100, Israel
(Received 3 June 1993; revised manuscript received 7 September 1993)

The intrinsic noise in the Couette-Taylor system with axial flow is evaluated experimentally by several methods, which include a comparison of experimental data with numerical simulations of the amplitude equation with a noise term and the application of an external source of stochastic perturbations at the inlet. The intensity of the intrinsic noise is found in our system to be dependent on the through-flow velocity in the following manner: for large enough through-flow velocities (Reynolds number $\mathrm{Re} > 2$) the intensity of the noise drastically increases with Re, whereas for small Re the noise amplitude is independent of Re and reaches a constant value of $\simeq 0.02$ μm/s, which is of the order of magnitude of the theoretically estimated value for the thermal noise. The amplitude of the intrinsic noise at large through-flow velocities ($\mathrm{Re} \simeq 3$) is found in our system to be larger than the thermal noise by more than one order of magnitude. Its origin is suggested to be associated with the perturbations of the flow at the inlet boundary.

PACS number(s): 47.20.−k, 47.60.+i, 43.50.+y

I. INTRODUCTION

The role of the intrinsic fluctuations in a pattern formation near the bifurcation point in systems far from equilibrium has been the subject of numerous theoretical and experimental studies for the past two decades [1–3]. Until very recently it was regarded that thermal fluctuations cannot play any significant role in pattern formation in hydrodynamical systems and that they are unobservably small due to the extremely small ratio between a microscopic thermal energy $k_B T$ and the macroscopic kinetic energy of hydrodynamical flows, e.g., in a convective roll $\rho d v^2$. The ratio between these values reaches usually 10–11 orders of magnitude, e.g., for Rayleigh-Bénard convection [3]. This conclusion was based on both theoretical estimates [1–3,5] and various experimental results [2,6–8]. The theoretical estimates suggested that in order to observe fluctuations of the velocity or temperature fields, which are caused by thermal fluctuations, on a macroscopic level, one should approach the close vicinity of the transition where the fluctuations grow enormously, similarly to the critical behavior in equilibrium systems. However, this suggestion was considered unrealizable experimentally due to various geometrical and thermal inhomogeneities existing in the real system, e.g., in thermal convection, such as thickness nonuniformity, imperfections due to finite-size effects, deviations from horizontality, various sources of thermal imperfections in convection, and experimental noise. These effects lead to a rounding of the transition, mask the role of fluctuations, and do not allow one to approach closely the transition point. Therefore a macroscopic fluid motion, caused by the imperfection and which existed before the transition, wipes out the contribution of the hydrodynamical fluctuations [6–8].

A new insight on the role of stochastic effects on pattern formation was obtained in Ref. [2]. The evolution of patterns in a thermal convection from the basic to the ordered state was studied under boundary conditions which eliminated the effects of sidewall forcing and provided evidence of the stochastic nature of the pattern formation process. However, a comparison of the data with solutions of model equations [5] gives the value of the noise intensity, necessary to fit the experiment, more than four orders of magnitude larger than the thermal noise in the Navier-Stokes equations. Therefore, the thermal noise fluctuations were ruled out as the driving force of the pattern formation in a stationary convection.

Nevertheless, it has been reported recently [9] that thermal noise fluctuations were observed and measured in electroconvection in nematic liquid crystals. This system has been shown to be particularly sensitive to noise. The effect of noise fluctuations is relatively larger because the elastic constant of a liquid crystal is small and because a layer of rather small thickness can be used. Electroconvection of traveling waves was observed in this system in the form of patches of weak convection rolls with randomly varying amplitudes. These patches were shown to be thermal noise fluctuations on the basis of a comparison with the stochastic Ginzburg-Landau (GL) equation. Measurement of intensity of the director fluctuations below the onset of electroconvection [10] also identified the origin of these fluctuations with the thermal noise.

The above-mentioned experiments were carried out in *absolutely unstable* and *absolutely stable* (electroconvection in liquid crystals) systems. A different approach to the measurement of thermal fluctuations is to study them in *convectively unstable* systems. In a convectively unstable system a small perturbation grows exponentially as it propagates downstream. The noise in the convectively unstable region therefore experiences an amplification process. When the system is sufficiently long, even a microscopic perturbation can be amplified to produce a macroscopic pattern downstream. Therefore convectively unstable system are more convenient to study experimentally the effect of hydrodynamical fluctuations in gen-

eral and thermal fluctuations in particular.

One example of a convectively unstable system exhibiting patterns which are possibly attributed to thermal noise is a quasi-one-dimensional ramped convection channel with a binary fluid mixture [11]. Patterns of very small amplitudes exhibiting an erratic spatiotemporal behavior were observed in this system. The patterns were interpreted as the amplification of the intrinsic thermal noise.

Another example of a convectively unstable system which exhibits noisy patterns is the Couette-Taylor system with an axial flow. This system has been shown [12–16] to be a very convenient system to study the convective amplification of noise. The noisy patterns are propagating Taylor vortices (PTV's) which exhibit a broad-peaked power spectrum [12,13] and in which the interface with the Couette-Poiseuille flow exhibits an irregular time dynamics [12]. Recently, Babcock, Ahlers, and Cannell [16] made an attempt to estimate the strength of the noise which drives the PTV's in this system. A comparison with numerical simulations of the stochastic GL equation suggested that the noise-sustained structures in the convectively unstable region of this system are the result of the thermal noise amplification [16].

The suggestion that the patterns in the convectively unstable region originate from the thermal noise implies that all other sources of noise except for the thermal one, such as fluctuations of the velocity field at the inlet, do not affect the system at all. This rather counter-intuitive statement motivated us to study in detail the intrinsic noise in our Couette-Taylor system with an axial flow in order to determine its intensity and possibly to determine its origin. It seemed to us that in an open flow system other noise sources, such as the perturbations that are initiated behind the mesh at the inlet, are much more effective than the thermal noise.

Several experiments were carried out in order to determine the intensity of the intrinsic noise, to be described in this paper. The main result is the following: for sufficiently large Reynolds number Re of the axial flow (Re > 2) the intrinsic noise in our system is not thermal, since its intensity increases with Re. It is found by several independent experiments that the magnitude of the intrinsic noise in our system reaches at $\mathrm{Re}\simeq 3$ a value which is more than one order of magnitude larger than the theoretical estimation for the thermal noise. At small Re, however, the intensity of the intrinsic noise exhibits a saturation at a value close to the estimated thermal noise level.

This paper is organized as follows. The theoretical estimates of the thermal noise are presented in Sec. II. The experiments to determine the strength of the natural noise in the Taylor system with an axial flow are described in Sec. III. The results are discussed in Sec. IV.

II. THEORETICAL ESTIMATES OF THE THERMAL NOISE

The theoretical estimations of the thermal noise that we were aware of were carried out for the Rayleigh-Bénard system. Following pioneering work of Zaitsev and Shliomis [1] and Graham [1], an expression for the thermal noise level was derived [3] for the two-dimensional Rayleigh-Bénard system [2], using the Swift-Hohenberg equation [5]. Babcock, Ahlers, and Cannell [16] converted it to the expression for the one-dimensional case, which is appropriate for the Couette-Taylor system with an axial flow. This system can be modeled by the complex Ginzburg-Landau equation (CGL) with a stochastic force $f(x,t)$

$$\tau_0(A_t+SA_x)=\bar{\epsilon}(1+ic_0)A+\xi_0^2(1+ic_1)A_{xx} -g(1+ic_2)|A|^2+f(x,t)\ , \tag{1}$$

where the complex force term obeys the correlation

$$\langle f^*(x,t)f(x',t')\rangle=\sigma_{\mathrm{th}}^2\delta(x-x')\delta(t-t')\ .$$

The coefficients of Eq. (1) for the radii ratio $\eta=0.75$ are [13,17] (up to very small correction due to Re) $\tau_0=0.0379$, $\xi_0^2=0.0725$, $S=1.23\,\mathrm{Re}$, and g is of the order unity. The complex coefficients c_0, c_1, and c_2 are very small and can be neglected. $\bar{\epsilon}$ is the distance from the convective line, defined as $\bar{\epsilon}\equiv[\Omega-\Omega_c(\mathrm{Re})]/\Omega_c(\mathrm{Re})$, where $\Omega_c(\mathrm{Re})$ is the critical rotation speed in the presence of an axial flow with a value of Re.

Babcock, Ahlers, and Cannell [16] suggested that the intensity of the noise fluctuations, denoted by σ_{th}^2, is given by

$$\sigma_{\mathrm{th}}^2=2\tau_0\left[\frac{\xi_0}{2k_c}\right]^{1/2}F_{\mathrm{th}}\ ,\quad F_{\mathrm{th}}=\frac{Pk_BT}{\rho d\nu^2}\ , \tag{2}$$

where P is the Prandtl number dependent prefactor typically of order 1, k_B is the Boltzmann constant, T is the temperature, ρ is the density, ν is the kinematic viscosity, and k_c is the critical wave number at the onset.

F_{th} is the ratio between the thermal energy and the kinetic energy $\rho V_d^2 d^3$ per volume d^3 with a vortex velocity $V_d=\nu/d$. For the parameters in our system, one gets $F_{\mathrm{th}}=4.7\times10^{-11}$ and $\sigma_{\mathrm{th}}=8.6\times10^{-7}$. The fact that F_{th} is so small explains why it is so hard to observe directly the thermal noise fluctuations.

In order to get an estimate for σ_{th} in dimensional (velocity) units, we use the relation between the noise power σ_{th}^2 and the zero-lag correlator $\overline{A}^2$, defined as the correlation function $\langle A(x,t)A^*(x+\Delta x,t+\Delta t)\rangle$ at zero lag $\Delta x=0$ and $\Delta t=0$ (A is the amplitude of the periodic underlying pattern). One finds [18]

$$\overline{A}^2=\frac{\sigma_{\mathrm{th}}^2}{4\tau_0\xi_0\sqrt{-\bar{\epsilon}}}\ . \tag{3}$$

The velocity fluctuations $\overline{V}_t^2$ are obtained from $\overline{A}^2$ by scaling with ν/d

$$\overline{V}_t^2=(2\pi)^2\left[\frac{\nu}{d}\right]^2\overline{A}^2\ . \tag{4}$$

We note that the prefactor $V_m=2\pi$ is specific to the geometry of a thermal convection with free-free boundary conditions and it may be different for our system.

For $\bar{\epsilon} \simeq 0.01$ we obtain

$$\hat{V}_t \equiv (\overline{V_t^2})^{1/2} = \frac{\nu}{d} V_m \frac{\sigma_{\rm th}}{2(\tau_0 \xi_0)^{1/2}(-\bar{\epsilon})^{1/4}} = 3.14\sigma_{\rm th} . \quad (5)$$

Substituting the value of $\sigma_{\rm th}$ we finally obtain for the thermal noise fluctuations, at $\bar{\epsilon} \simeq 0.01$, $\hat{V}_t \simeq 0.027$ μm/s. We would like to emphasize that this value is a rough estimate and can be changed due to, first, a different prefactor in Eq. (4) (which, as will be shown later, is about 1.5 times less in our experiment), and second, a different prefactor in Eq. (2) in the relation between $\sigma_{\rm th}$ and $F_{\rm th}$. Both prefactors can reduce the estimated value for $\hat{V}_t$ up to an order of magnitude [19].

III. EXPERIMENTAL ESTIMATES OF THE INTRINSIC NOISE

A. Experiment

The experimental setup consists of the Taylor column, the axial flow modification, and the Laser Doppler anemometer (LDA), which was the main measuring tool. The details of the design are described elsewhere [14,15]. The column that was used in the experiments has an aspect ratio of $\Gamma = L/d = 48$ (L is the length of the working-fluid region), and radii ratio $\eta = r_1/r_2 = 0.77$. The radii of the outer and inner cylinder were $R_2 = 4.100$ and 3.150 cm, respectively.

The column was installed horizontally and was modified by the axial flow arrangement. The axial flow was driven by gravity in a closed loop, with the use of a pump. The average flow rate was measured by precise flow meters (Rota Model Nos. L63 and L6.3) in the range from 2×10^{-3} to 1.5 cm/s with an accuracy of 1×10^{-4} cm/s. In order to make the axial flow as uniform as possible in the azimuthal direction, the fluid passed an inlet chamber before entering the working region between the cylinders. The inlet chamber was constructed with flow directors and a stainless-steel net with (0.25×0.25) mm^2 mesh size. The net was used as nonrotational lateral boundaries at both sides of the column. The working fluid was a mixture of glycerol in water. Typically, the fluid had a kinematic viscosity of $\nu = 3.0cS$, which corresponds to a mixture of 32.4% by volume of glycerol in water at 22 °C. The viscosity of the fluid was determined from tabulated data [20] and was checked by measurements with a commercial viscometer (Haake CV-100). The temperature of the fluid was maintained constant to a level of ±25 mK. The temperature stability was achieved by circulating water in a jacket around the volume by the use of a commercial refrigerator-heater circulating system (Lauda RM6) and by stabilizing the room temperature to within ±1 °C. Before entering the column, the fluid passed through a copper tube which was immersed in the circulator water basin, so that the axial flow was stabilized to the desired temperature at the inlet.

The angular velocity of the inner cylinder was controlled by a stepper motor (Slo-Syn, model MO62-FD09) via a semirigid coupling. The motor was driven by a homebuilt electronic driver controlled by a computer.

B. Noise-sustained structures in the Couette-Taylor system with an axial flow

The Couette-Taylor system with an axial flow is governed by two control parameters. The first is the reduced rotation speed of the inner cylinder $\epsilon \equiv (\Omega - \Omega_0)/\Omega_0$, where Ω_0 is the rotation speed for the onset of the Taylor vortices without axial flow and ϵ is related to $\bar{\epsilon}$ in Eq. (1) through $\bar{\epsilon} = (\epsilon - \epsilon_c)/(1+\epsilon_c)$. The second parameter is the Reynolds number of the velocity of the axial flow $\mathrm{Re} = \bar{V}d/\nu$, where $\bar{V}$ is the averaged throughflow velocity and d is the gap size.

The stability diagram for the PTV's is shown in Fig. 24 in Ref. [14], which will be referred to below as I. The lower dashed line in this figure is the theoretical curve for the onset of a convective instability [13,17] $\epsilon_c = 0.000\,381\,\mathrm{Re}^2$. The upper solid line is the theoretical absolute instability line [13,17], $\epsilon_a = 0.007\,89\,\mathrm{Re}^2$, above which the flow is absolutely unstable (region III). The solid circles correspond to ϵ_s, which denotes the experimental observation [12,14] for the PTV's onset, measured at $L = 40d$. The data points determine the boundary between region I, where no patterns are present, and region II, where the PTV's are observed. Note that for $\mathrm{Re} > 1$, $\epsilon_s < \epsilon_a$, which implies that patterns exist in the convectively unstable region. The patterns that exist in the convectively unstable region were shown [12–14,16] to be the noise-sustained structures (NSS's). The effect of noise on the PTV's in the convectively unstable region is manifested in two ways [12–14]. The first manifestation is irregular fluctuations of the interface separating the PTV's from the Couette-Poiseuille flow and the second one is a broadband in the power spectrum. The PTV's state in the absolutely unstable region [12–14], on the other hand, exhibits a stationary interface between the PTV's and the Couette-Poiseuille flow, and a sharp peak in the power spectrum.

The interface between the PTV's and the Couette-Poiseuille flow in the convectively unstable region is presented in Fig. 17 in I. The solid line across the plot defines the interface position [12,14]. The irregular fluctuations of the interface give rise to a random modulation of the velocity amplitude of the PTV's, as shown in Fig. 16 in I, where time series of the PTV's velocity in the convectively unstable region in the vicinity of the interface for two values of the through-flow velocity [$\mathrm{Re} = 2.74$ in (a) and $\mathrm{Re} = 1.55$ in (b)] are presented. The mechanism that generates the NSS's in the convectively unstable region was identified [12–14] as a continuous process of amplification of the intrinsic noise in the system. It is our goal to evaluate the intensity of this intrinsic noise in our system.

C. Difficulty of the direct measurement

A direct measurement of the natural noise in the system is quite difficult to perform. One might try to estimate the natural noise of the system by a direct measurement of the velocity fluctuations just behind the inlet boundary. This approach is rather difficult to carry out, because of a deficiency of the LDA, namely, the broadening of the peak in the frequent spectrum of the scattered

signal due to the flow. This broadening is inherent to LDA and can be explained in the following manner. The scattering particles arrive at random times to the measuring volume and the phase fluctuations in time are manifested by frequency fluctuations of the LDA signal. It was shown [21] that the contribution of many particles arriving with random phases results in a Gaussian spectrum with a standard deviation which is linearly proportional to the velocity of the flow. The broadening of the peak in the frequency spectrum of the optical signal corresponds directly to an uncertainty in the velocity measurement. Therefore, when measuring a fluctuating velocity field, one must take into account the contribution of the fluctuations which are due to the LDA. Velocity fluctuations which were recorded by the LDA are presented in Fig. 1 as a function of Re of the Poiseuille flow. These velocity fluctuations are composed of both the inherent LDA fluctuations *and* the fluctuations due to the intrinsic noise of the system. No spatial dependence of the measured velocity fluctuations was observed. Figure 1 shows that at $\mathrm{Re}=1.0$, a value for which the noise-sustained structures just start to be observable [12], the measured fluctuations reach a value of about 50 μm/s, or rms velocity of about 17 μm/s, which is about three orders of magnitude larger than the estimated thermal noise. Therefore, it is clear that the dominant contribution to the measured fluctuations are the fluctuations which are due to the LDA. Figure 1 also shows that the amplitude of the measured fluctuations increases approximately linearly (within the error bars) with Re, as expected from fluctuations which are due to the LDA. In view of the above considerations, it was clear that the natural noise in the system should be measured indirectly.

D. Numerical simulations of the CGL equation

An important tool in the study of the origin of noise in the system was the development of a numerical simulation of the model equation. Numerical simulations of the CGL equation (1) were carried out in order to examine the effects of the noise on the onset of the patterns in the convectively unstable region.

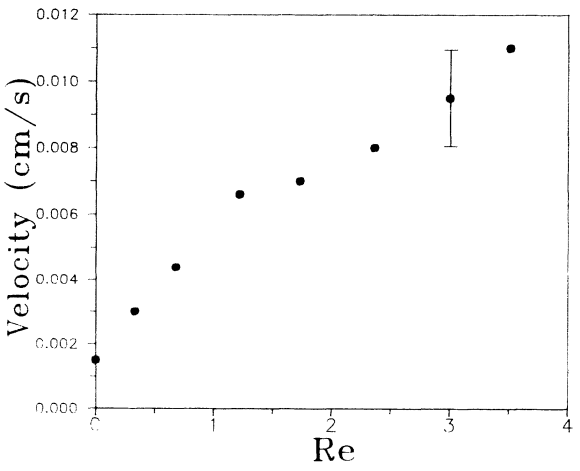

FIG. 1. The peak-to-peak axial velocity fluctuations behind the inlet boundary vs Re, without rotation of the inner cylinder. These fluctuations result from both intrinsic noise fluctuations and the inherent broadening of the LDA signal.

Two methods were used in order to model the noise. The first corresponds to a "boundary noise," namely, random values were chosen for the real and imaginary parts of the amplitude at the point $x=0$, at each time step. The random values were chosen either from a Gaussian distribution with a standard deviation σ_n, or were distributed uniformly between $\pm n$. n, or σ_n, represents the noise level. They are related by $\sigma_n^2=n^2/3$. The noise level was scaled with time by multiplication with $1/\sqrt{\Delta t}$, where Δt is the interval between time steps. The choice of the $x=0$ point as the source of the noise was motivated by the fact that the mesh at the inlet serves as a source of perturbations. Moreover, a perturbation that is generated at the inlet has more time to develop along the column, so the contribution of the inlet is more significant than the contribution of other points in the column.

The second method corresponds to a "volume noise." A stochastic complex term, denoted by f, was added to the right-hand side of Eq. (1) to take into account the noise in the system. f has the properties

$$\begin{aligned}\langle f(x,t)\rangle &= \langle f(x,t)f(x',t')\rangle \\ &= \langle f^*(x,t)f^*(x',t')\rangle = 0 , \\ \langle f^*(x,t)f(x',t')\rangle &= \sigma_n^2\delta(x-x')\delta(t-t') .\end{aligned} \tag{6}$$

The stochastic GL equation was integrated numerically by an explicit scheme [22].

In order to compare the two methods by which the noise can be introduced into the CGL equation, the interface position L_h between the PTV's and the Couette-Poiseuille flow was determined in the numerical simulation for different values of the noise level, for the boundary noise and for the volume noise. The results of the simulations are shown in Fig. 2, which presents L_h vs the noise level σ_n. The open and solid circles correspond to the averaged value of L_h in the presence of the boundary noise and the volume noise, respectively. It is seen that the boundary noise is slightly more effective than the volume noise because the value of L_h that correspond to the boundary noise is smaller than the value that corresponds to the volume noise, for a given noise level. This observation is somewhat surprising since it means that the noise which is generated at only one spatial point, the inlet boundary, has a greater effect than the noise that is generated throughout the entire system. This numerical observation was also confirmed by Deissler [23]. We note, however, that, although data that corresponds to the boundary noise lies below the data that correspond to the volume noise consistently for the whole range of σ_n, the two data sets are separated from each other by approximately one unit of d. This separation is smaller than the spatial size of the fluctuations around L_h, which is about one to two units of d. Although in principle such a difference can be resolved by sufficient time averaging, in practice the difference between the two ap-

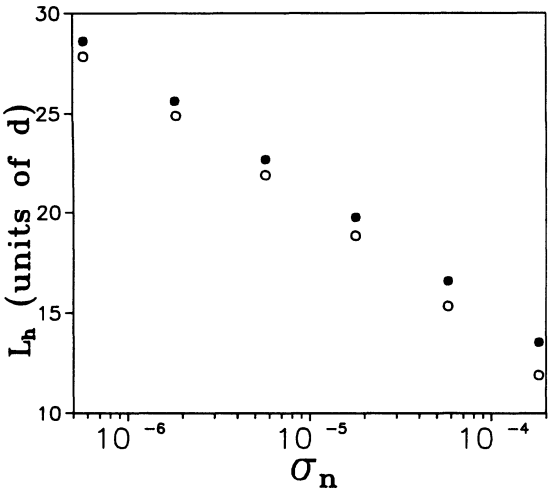

FIG. 2. The interface position L_h vs the noise level σ_n, as calculated in the numerical simulations, for boundary noise (open circles) and volume noise (solid circles). Re=3.41 and $\bar{\epsilon}=0.05$.

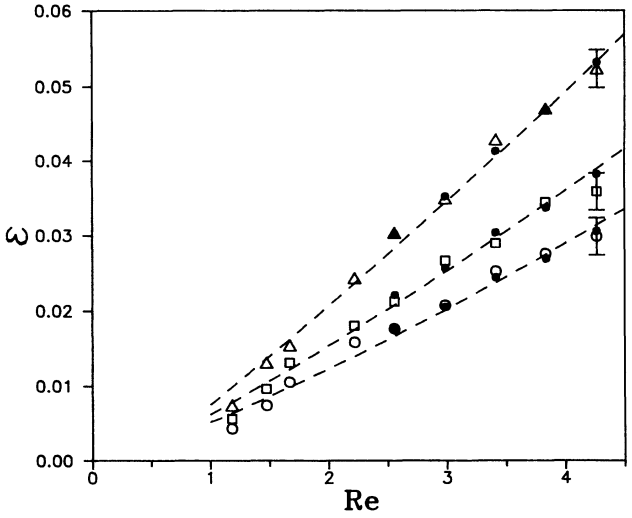

FIG. 3. The pattern onset ϵ_s vs Re for different aspect ratios. The open symbols denote the experimental observation for the pattern onset at $\Gamma=20$ (triangles), 30 (squares), and 40 (circles). The dashed lines are the result of the fit by Eq. (7). The solid circles denote the result of numerical simulations of the stochastic CGL equation with $\sigma_n=1.2\times10^{-5}$.

proaches to too small to be important in our study. For convenience, the boundary noise method was chosen to be used in the simulations.

E. Onset of patterns

Numerical simulations of the CGL equation were carried out in order to determine the position of the interface between the PTV's and the Couette-Poiseuille flow at a given Re for various values of ϵ. The interface position was determined, similar to the experiment [12,14], at a point where the amplitude decayed to 10% of its saturation value. The results of the simulations were compared to the experimental data for ϵ_s, corresponding for the PTV's onset, as a function of Re and downstream distances z/d (changing z/d is equivalent to changing the aspect ratio Γ). The experiment was carried out as following: for a given Re value, Ω was increased quasistatically from below $\Omega_c(\mathrm{Re})$. At each Ω the axial velocity was measured as a function of time with the LDA. Before measuring we waited sufficient time in order to let the convective patterns advect away. This waiting time was typically several horizontal traverse times $\tau=(\Gamma/\mathrm{Re})\tau_v$ where $\tau_v=d^2/\nu$ is the viscous diffusion time.

The experimental data and the results of the simulations are presented in Fig. 3. The open symbols correspond to the experimental data (circles, squares, and triangle correspond to downstream distances of $z/d=40$, 30, and 20, respectively) and the solid circles correspond to the numerical simulations. The dashed lines correspond to a fit of the experimental data to the following equation [24], which gives the relation between the onset of the patterns and the values of Γ and S

$$\bar{\epsilon}_s=\tau_0\Gamma^{-1}S\ln\gamma-\left[\frac{\xi_0}{\Gamma}\ln\gamma\right]^2. \tag{7}$$

Equation (7) is derived by solving the linear part of the CGL equation (1). The parameter γ is defined as the ratio between the perturbation initial amplitude and the amplitude of the pattern at $z=\Gamma$, where the onset of patterns takes place. The fit to the experimental data yields [14] $\gamma=181$. (We note that Babcock, Ahlers, and Cannell [13] obtained in a similar procedure, however, at onset and not at 10% of saturation as we did here, a value of $\gamma=590$ for their data and for $\Gamma=100$.) The value of σ_n that matches the experimental data, in the range $2.5<\mathrm{Re}<4.5$, was found to be $\sigma_n=1.2\times10^{-5}$. If we assume that the same ratio between the velocity fluctuations $\hat{V}_0$ and the noise strength σ_n as in Eq. (5) holds, then one obtains from Eq. (5) $\hat{V}_0=0.38$ μm/s. Both values for σ_n and $\hat{V}_0$ are larger by more than an order of magnitude than the estimated value for the thermal noise. Since the results of the fit either by Eq. (7) or by the numerical simulations of Eq. (1) is a one parameter fit (γ or σ_n), the estimated level of the intrinsic noise turns out to be independent of Re in the range $2.5<\mathrm{Re}<4.5$. A different experiment shows below that the noise is strongly dependent on Re in this range. This insensitivity may be explained by the fact that only one point on the interface was used to fit the data.

F. Experiments with external noise

A different approach to obtain the intensity of the intrinsic noise was to introduce an external source of noise with a variable intensity to the system and to measure its effect on the PTV's in the convectively unstable region. Our objective was to deduce the intensity of the intrinsic noise from the extrapolation to a zero value of the external noise amplitude. In order to examine experimentally the effect of noise on the system, we have used the motion of the inlet lateral boundary as a source of perturbations. The motivation for the choice of the inlet stems from our

assumption that the experimental noise of the system is generated mainly at the inlet boundary. Moreover, a perturbation that is generated at the inlet has more time to be amplified as it propagates downstream than one generated at any other point along the column, and therefore the inlet is more significant to the generation of the NSS's.

The intrinsic noise of the system is random in nature. In order to produce a random perturbation which imitates the natural noise, an axial motion of the inlet boundary was activated by a random signal, generated by a computer. The boundary, a stainless-steel ring with a mesh of 0.25^2 mm^2 grid size, was connected by two rods to a stepper motor. The motor was driven by pulses applied by a random number generator routine. In each pulse the motor was activated for a number of steps n, that was distributed uniformly between 0 and some specified number $n_{\max}$, back and forth. $n_{\max}$, which determined the amplitude of the generated perturbation, corresponded to a traverse distance of $n_{\max}/200$ mm of the inlet boundary. The frequency of the steps was 333 Hz, which corresponds to a velocity of the inlet boundary of 1.67 mm/s. A typical spectrum of the function $n(t)$, for $n_{\max}=300$, is shown in Fig. 4, where $P(f)$ is the square root of the power spectrum. We used as a measure of the noise level the averaged value of the spectrum $P(f)$, which will be denoted by $\bar{P}(f)$. There is a linear relationship between $\bar{P}(f)$ and $n_{\max}$, as shown in Fig. 5. This choice of quantifying the noise level is arbitrary, and in the following we will discuss the way by which $\bar{P}(f)$ was related to physical units. The time between pulses was also random, so that the generated perturbations will not be correlated, and was distributed uniformly between 0 and $0.92/f_0=19.3$ s, where f_0 is the frequency of the PTV's for the specific Re of the experiment, namely, Re=3.0. The measured axial velocity near the inlet boundary is presented in Fig. 6, in the presence of the

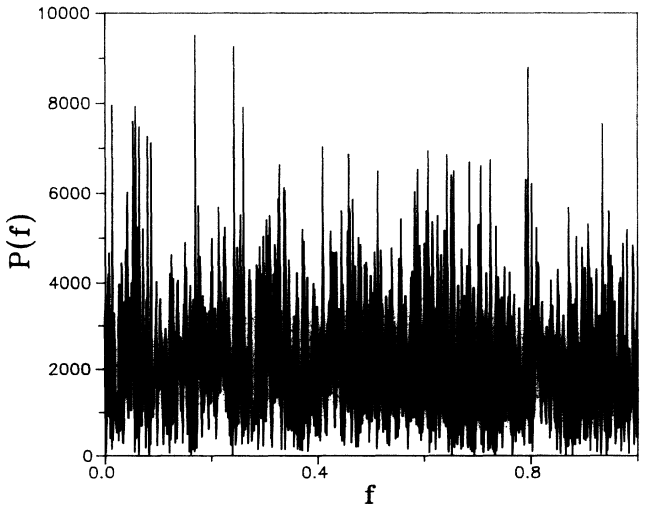

FIG. 4. The square root of the power spectrum of a sample of 1024 numbers, between 0 and $n_{\max}=300$, that are chosen by a random number generator routine. The f axis was normalized to be between 0 and 1.

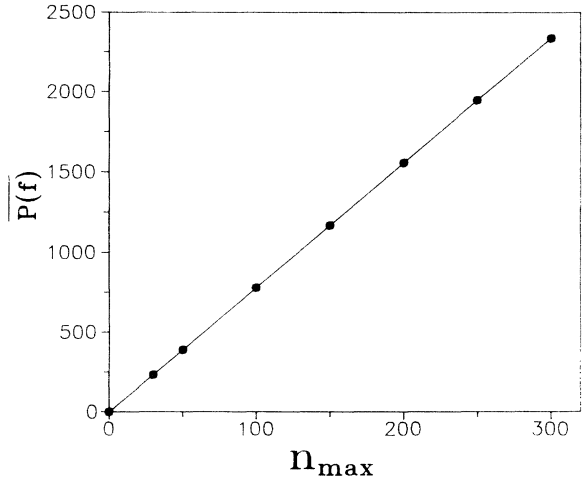

FIG. 5. $\bar{P}(f)$, the averaged value of the spectral amplitude, vs $n_{\max}$. The slope is 7.786.

mechanical noise with $\bar{P}(f)=2141$. As is seen from this figure, the mechanical noise generates perturbations with a random amplitude, which correspond to the observed "spikes" with random peak-to-peak velocities values. The power spectrum of the measured axial velocity is presented in Fig. 7. It seems to be uniform in a wide range of frequencies.

The following experiment was carried out. For fixed Re and ϵ, the mechanical noise was applied to the system, at several values of the noise level $\bar{P}(f)$. $\bar{P}(f)$ was in the range between 234 and 2335 ($30<n_{\max}<300$). For each $\bar{P}(f)$ value the position of the interface between the PTV's and the Couette-Poiseuille flow was determined by an analysis of the pictures of the PTV's state that were grabbed with the vidicon camera. In order to determine the interface position several methods were used [12,14]. One method that was used in the analysis is the demodulation of the optical signal in order to eliminate the fast oscillations and to obtain the profile envelope. The inter-

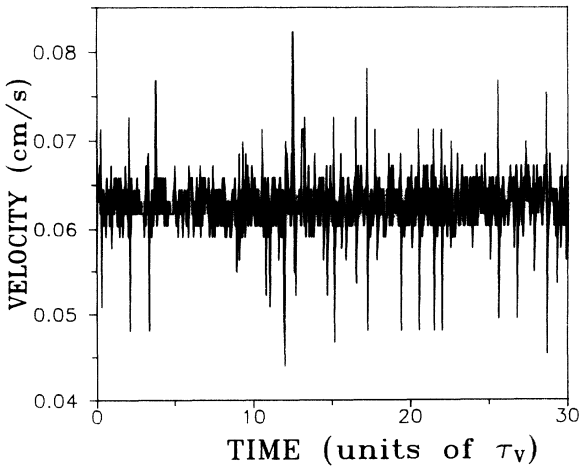

FIG. 6. The axial velocity measured near the inlet boundary in the presence of the mechanical noise with $\bar{P}(f)=2141$, vs time, for Re=3.0 and without rotation.

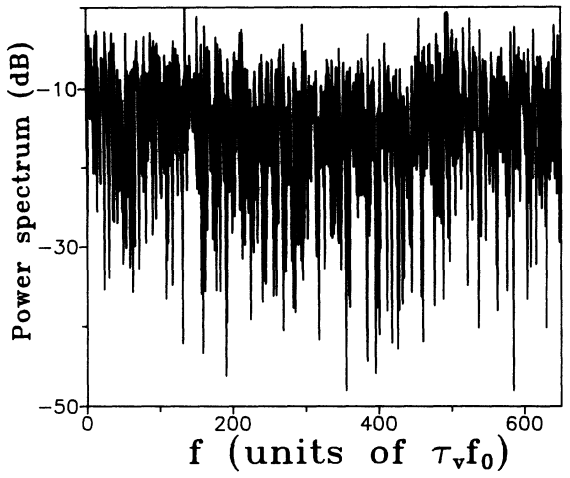

FIG. 7. The power spectrum of the velocity shown in the preceding figure. The frequency is nondimensionalized by scaling with the PTV's frequency $f_0=0.0478$ Hz.

face position was determined as the point that corresponds to a value of the demodulated amplitude larger than some specified threshold. We used in the analysis also root mean square (rms) and integral methods, namely, the threshold was set to be a specified fraction of either the root mean square value of the velocity of the PTV's near the outlet, or a fraction of the integral over the rms velocity along the column. The latter specification of the threshold was mainly used because it is less sensitive to spurious intensity variations.

The values of L_h as a function of $\bar{P}(f)$ for $\bar{\epsilon}=0.034$ at Re=3.0 are shown in Fig. 8. The circles are the data and the solid line is a logarithmic fit. The dashed line is a result of numerical simulations of the stochastic GL equation with the boundary noise of strength σ_n. In the simulations the interface position was determined for given Re and $\bar{\epsilon}$, and for different values of the noise strength σ_n. The interface was determined, as in the experiment, at the point where the velocity amplitude was decreased to 10% of the saturation value. The dashed line is only a part of the data obtained in the simulations. The complete $L(\sigma_n)$ data set is presented in Fig. 9.

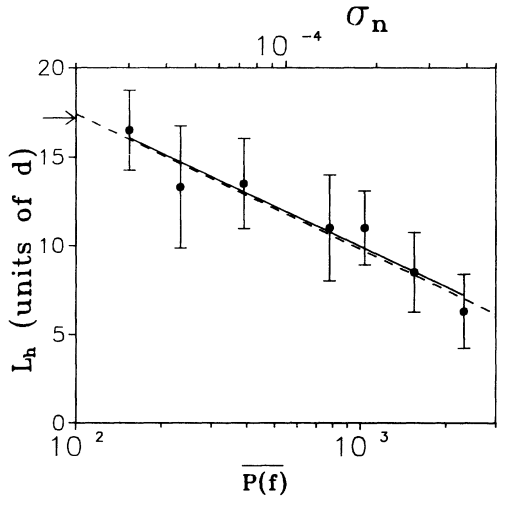

FIG. 8. The interface distance from the inlet L_h vs the strength of the external noise, for Re=3.0 and $\bar{\epsilon}=0.034$. The circles correspond to the experimentally measured L_h vs $\bar{P}(f)$ and the solid line is a logarithmic fit to the data. The dashed line correspond the numerical simulations of L_h vs σ_n, obtained from the numerical simulations. The arrow at $L_0=17.2d$ indicates the value of L_h measured without external noise. The value of σ_n that corresponds to L_0 is $\sigma_{n,0}=2.1\times10^{-5}$

It is seen from Figs. 8 and 9 that the noise level determines the position of the interface between the Couette-Poiseuille flow and the PTV's. Increasing the noise results in perturbations with larger initial amplitude, which grow to produce a pattern with an interface positions at a shorter distance from the inlet. The interface position without mechanical noise was measured to be at $L_0=17.2d$, at the arrow's position in Fig. 8. The distance L_0 corresponds to a noise level with a value of $\bar{P}(f)=\bar{P}_0(f)$, which is equivalent to the natural noise in the system. From the comparison of the experimental data and the numerical simulations we obtain two things. First, the arbitrary units of $\bar{P}(f)$ can be scaled with the units of σ_n, which are related to the noise more directly. On the basis of this data and the data with $\bar{\epsilon}=0.029$ we can find a relation between $\bar{P}(f)$ and σ_n. Second and more important, we find that the intrinsic noise in the system corresponds to $\sigma_n=2.1\times10^{-5}$, for $\bar{\epsilon}=0.034$. A similar comparison for $\bar{\epsilon}=0.029$ yields $\sigma_n=1.2\times10^{-5}$. The plot of L_h vs $\bar{P}(f)$ and σ_n for this $\bar{\epsilon}$ is shown in Fig. 10. The velocity fluctuations estimated from σ_n and the relation (5) is on average $\hat{V}_0=0.52\ \mu$m/s.

In conclusion, the estimated value of the natural noise is close to the value obtained in Sec. III E. We note that this experiment was carried out at Re=3.0. A different procedure to measure the velocity fluctuations of the intrinsic noise is described in Sec. III G.

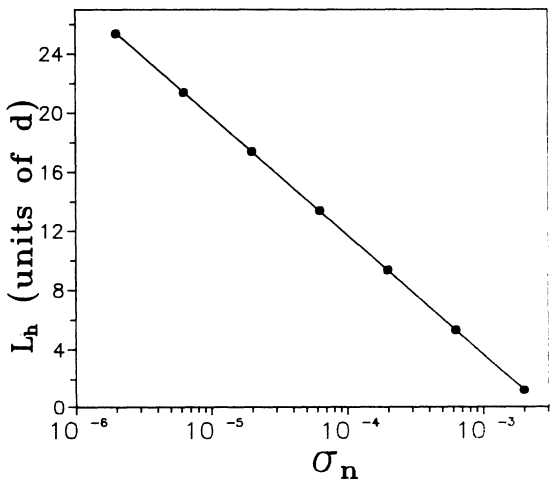

FIG. 9. The interface position L_h vs σ_n from the numerical simulations, in a wide range of the noise amplitude, for Re=3.0 and $\bar{\epsilon}=0.034$. The circles are the calculated data and the solid line is a logarithmic fit.

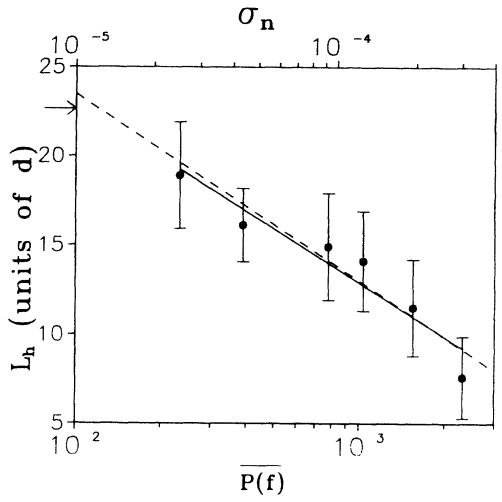

FIG. 10. The interface distance from the inlet L_h vs the strength of the external noise, for Re=3.0 and $\bar{\epsilon}=0.029$. The symbols are the same as in Fig. 8. In this case $L_0=22.7d$ and $\sigma_{n,0}=1.2\times10^{-5}$.

G. Noise evaluation from the PTV's profile

The existence of the PTV's in the convectively unstable region is due to the continuous intrinsic noise, whose main source is assumed to be the inlet boundary. An increase of the boundary noise, for example, by mechanical means as described above, shifts the interface between the Couette-Poiseuille flow and the PTV's towards the inlet, as shown above. Since a given noise intensity at the inlet determines the position of the interface, one can in principle deduce the noise intensity at the inlet from the value of the interface distance from the inlet. In order to put this principle into practice we carried out the following procedure. First, a measurement of the spatial profile of the PTV's state in the convectively unstable region was carried out. Then the data for the velocity amplitude was fitted to the solution of the GL equation and the velocity amplitude at the inlet was obtained from the fit. There are two possibilities to carry out this procedure. First, one can use the stochastic time-dependent GL equation (1) to fit the data, and, second, one can use the stationary deterministic GL equation to fit the experimental spatial profiles of the PTV's. The latter method follows from the obvious observation that at a given value of the noise intensity at the inlet the time dependence of the interface results just in a noisy modulation of the velocity amplitude around an averaged stationary profile. The longer averaging, the closer to the stationary averaged profile. Therefore, by averaging Eq. (1) for a long enough time one gets the stationary GL equation for the rms real amplitude B

$$\tau_0 S B' = \bar{\epsilon} B + \xi_0^2 B'' - g B^3 , \tag{8}$$

where prime indicates differentiation with respect to x. (The complex terms are negligibly small and therefore were not considered in the equation.) The value of the velocity amplitude at the inlet boundary, which corresponds to the intrinsic noise at the inlet, can then be deduced from the fit by a procedure that is outlined in the Appendix.

1. PTV's profile with external noise

We first carried out an experiment in which Re and ϵ were constant and the level of an external noise was varied. For given Re=3.06 and $\bar{\epsilon}=0.034$ and for various values of the external perturbation ($n_{\max}=100$, 150, 200, and 250 which correspond to $\bar{P}(f)=779$, 1168, 1558, and 1947, respectively) the velocity amplitude along the column was measured and fitted to the solution of the GL equation, by the following procedure. At every spatial point the velocity was recorded as a function of time for a period of time long enough to observe the velocity amplitude modulations. (This period of time was typically $30/f_0$, where f_0 is the PTV's frequency.) At every spatial point the rms value of the amplitude, found from the velocity time series, was taken as a data value which corresponds to this point along the profile. The data for the velocity amplitude was fitted to Eq. (8).

A typical plot of the profile is shown on Fig. 11, for which $\bar{P}(f)=1947$. The solid circles are the measured data and the solid line is the result of the fit. For each profile the interface position L_h (the distance for which the amplitude reaches 10% of its maximum value) was measured. A plot of the L_h as a function of the velocity amplitude at the inlet $\hat{V}_0$ is shown on Fig. 12. The circles are the measured points and the solid line is a logarithmic fit to the data. The arrow points out the value L_0 of the interface position which corresponds to the profile associated with the PTV's state with the same Re and $\bar{\epsilon}$, namely, Re=3.06 and $\bar{\epsilon}=0.034$, and without an external mechanical noise. Extrapolating the fitted line to L_0 gives that the value of the velocity amplitude of the intrinsic noise is $\hat{V}_0=0.24$ μm/s. The relation between $\hat{V}_0$ and the value of σ_n (that was found in the experiment described in the previous section and was carried out at the

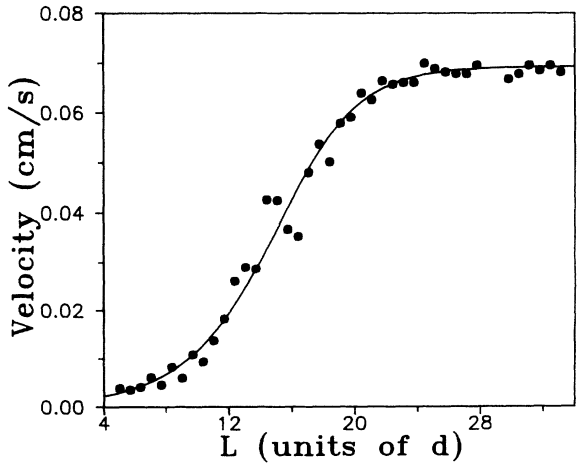

FIG. 11. The velocity amplitude of the PTV's vs distance from the inlet for Re=3.06 and $\bar{\epsilon}=0.034$, with external noise of $\bar{P}(f)=1947$. The solid line is a fit to the GL equation. The fit gives for the rms velocity amplitude at the inlet $\hat{V}_0=8.06$ μm/s.

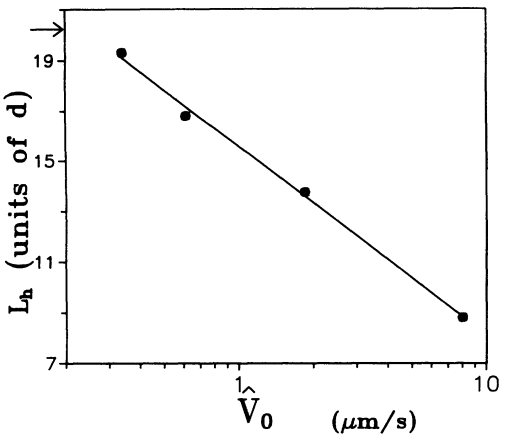

FIG. 12. The interface position L_h vs the velocity amplitude of the external noise at the inlet, deduced from the fits to the GL equation. The circles are the data and the solid line is a logarithmic fit. The arrow points out the interface distance that corresponds to the profile without external noise, for which $\hat{V}_0=0.24\ \mu$m/s (Re=3.06 and $\bar{\epsilon}=0.034$).

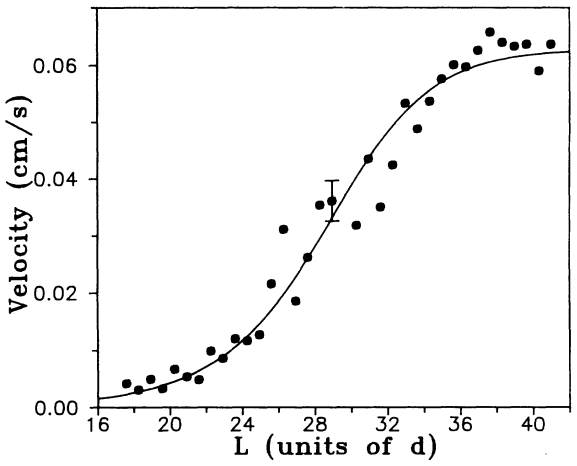

FIG. 13. The velocity amplitude vs the distance from the inlet for Re=3.5 and $\bar{\epsilon}=0.0367$, without external noise. The solid line is a fit to the GL equation. The fit gives for the velocity amplitude at the inlet $\hat{V}_0=0.27\ \mu$m/s. A typical error bar is shown.

same Re) gives an experimental analog of Eq. (5)

$$\hat{V}_0=1.45\sigma_n\ . \tag{9}$$

The different prefactor is probably explained by the fact that the relation (5) was obtained for the Raleigh-Bénard convection with free-free boundaries. Thus, if one takes the relation (9) instead of (5), the estimated value for the velocity amplitude due to the thermal fluctuations at $\bar{\epsilon}\simeq 0.01$ will be $\hat{V}_t\simeq 0.013\ \mu$m/s.

2. *PTV's profile without external noise*

A different experiment that was based on the same measurement procedure was to vary Re without applying an external noise to the system. This experiment allows us to find dependence of the noise intensity on the through-flow velocity in a relatively simple and direct procedure.

The measurement procedure was the following: for given Re and ϵ we measured the spatial velocity profile of the noise-sustained structures in the convectively unstable region. Re was set to the desired value and $\epsilon<\epsilon_a$ was tuned to obtain a spatial profile which had an interface position at about half of the column's length. A typical plot of the measured velocity amplitude and the corresponding fit to Eq. (8) is shown on Fig. 13 for Re=3.5 and $\bar{\epsilon}=0.0367$. The circles correspond to the data and the solid line is the fit resulting from the numerical solution of Eq. (8). The fit in this case gives for the rms value of the noise at the inlet $\hat{V}_0=0.27\ \mu$m/s. The procedure of the velocity amplitude measurements and fitting to the GL equation was carried out for various values of Re. A plot of the velocity amplitude of the fluctuations $\hat{V}_0$ vs Re is shown in Fig. 14. At large enough through-flow velocities (Re>2) the intensity of the noise increases with Re. For small through-flow velocities, however, the intensity of the noise is saturated at a value of $\hat{V}_0\simeq 0.02\ \mu$m/s, which is close to the thermal noise level, according to our rough estimate. This dependence of $\hat{V}_0$ on Re suggests that in our system the intrinsic noise is not thermal for large Re. It has probably a hydrodynamic origin and is produced by the mesh at the inlet boundary. For small Re, however, the perturbations become small enough and reach a level which is comparable with the thermal fluctuations. We would like to stress again that the noise level at the inlet increases about 15 times when Re increases from about 2 up to 3.5.

IV. DISCUSSION

Several methods of the experimental determination of the intrinsic noise intensity in our system were presented above. These methods took advantage of the fact that the convectively unstable region is very sensitive to noise, so that patterns of macroscopic size are generated in a process of noise amplification.

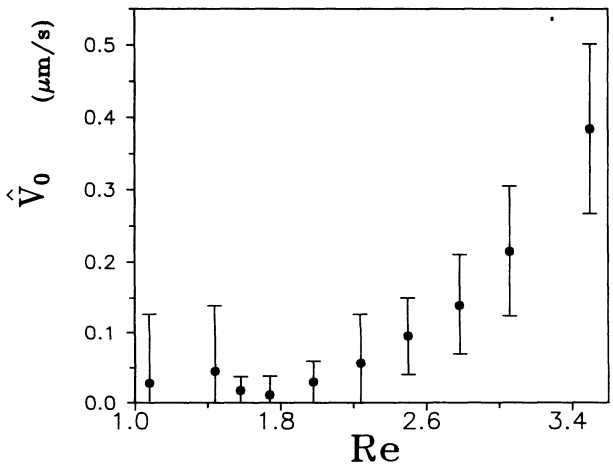

FIG. 14. The rms velocity amplitude at the inlet, deduced from velocity profiles without external noise, vs Re.

The first method that was described above was based on a comparison between the experiment and numerical simulations of the GL equation with a stochastic force, for the onset of the NSS's in the convectively unstable region, in the range of $2.5 < \mathrm{Re} < 4.5$. The analysis gives for the noise fluctuations $\sigma_n = 1.2 \times 10^{-5}$ that corresponds to the velocity amplitude $\hat{V}_0 = 0.17$ μm/s, according to Eq. (9). This method is based on the fit of the experimental data and numerical simulations at one point on the spatial profile, namely, the point where the amplitude reaches 10% of its saturation value. This method is not sensitive to the dependence of the noise level on Re.

A different method, which was carried out at $\mathrm{Re} = 3.0$, was based on the comparison between experiments and numerical simulations to find the interface position as a function of an external noise intensity. This method yielded after extrapolation $\sigma_n = 1.65 \times 10^{-5}$ in average, which corresponds to a noise level of $\hat{V}_0 = 0.24$ μm/s, according to the relation (9). This method has also the disadvantage of comparing the data and the simulations at only one point on the profile at different values of the noise level.

We then presented another method to deduce the noise level at the inlet boundary. This method was based on the fitting of measured full velocity profiles along the column to the GL equation. Measurements of velocity profiles at several external noise levels and at a fixed $\mathrm{Re} = 3.0$ were first carried out. An extrapolation to zero external noise yielded for the intrinsic noise fluctuations at $\mathrm{Re} = 3.0$ a value of $\hat{V}_0 = 0.24$ μm/s.

The most important result was obtained from the measurements of velocity profiles along the column without external noise at different Re values. This method to deduce the intensity of the intrinsic noise in the system is based on the detailed measurement of the rms velocity profile. An evidence for two different sources of noise was discovered by this method in our system. It was found that there is a crossover at $\mathrm{Re} \simeq 2$, below which the intensity of the intrinsic noise is saturated at a constant noise level independent of Re and above which the noise fluctuations drastically increase with Re. The amplitude of the noise reaches at $\mathrm{Re} = 3.0$, a value which is more than an order of magnitude larger than the theoretical estimation for the thermal noise. The latter result is supported by several different experiments carried out at larger Re and described above. The origin of the noise at large Re can be attributed to the perturbations of the flow which are generated behind the mesh at the inlet boundary. At $\mathrm{Re} \simeq 2$ the intensity of the noise reaches a level which is close to the thermal noise. We would like to stress here the importance of the possibility to deduce information on the microscopic noise fluctuations from measurements of macroscopic structures.

As was pointed out above, it was found in the numerical simulations that the boundary noise is more effective than the bulk noise. The inlet boundary is therefore the most important source of noise for large Re. By changing Re one can tune the noise level in the system down to the microscopic level at small Re. We note that the saturation value of the noise at small Re is $\hat{V}_0 \simeq 0.02$ μm/s, which is about the theoretical estimation for the thermal noise $\hat{V}_t \simeq 0.013$ μm/s, according to the relation (9). (We are aware of the fact that the calculation of the thermal noise was based on the Rayleigh-Bénard convection, and therefore a correction by some numerical factors for the Couette-Taylor flow can be expected [19]). We note that Babcock, Ahlers, and Cannell [13,16] have found in their Coutette-Taylor apparatus that the intrinsic noise at $\mathrm{Re} = 3$ was at the thermal noise level. It is conceivable that the value of Re at which the intrinsic noise reaches the thermal level is not universal and depends on the particular apparatus.

ACKNOWLEDGMENTS

We acknowledge helpful discussion and correspondence with J. P. Eckmann, R. J. Deissler, and M. Lücke. This work was partially supported by the U.S.–Israel Binational Scientific Foundation Grant No. 90-00412, the Israel Science Foundation Grant No. 425/90-2, and the German-Israel Foundation Grant No. I-130091.

APPENDIX: DATA FITTING WITH THE SOLUTION OF GL EQUATION

First we wish to justify the use of the stationary GL equation (8). We note that indeed the profile of the PTV's state is not stationary, as was demonstrated elsewhere [14]. The time-dependence of the interface results in modulations of the velocity amplitude along the profile. This, however, merely causes a larger scatter of the profile measurement data. The typical measured profiles that are shown in Figs. 11 and 13 demonstrate that the interface fluctuations do not influence the shape of the profile too much. Therefore, the stationary GL equation, Eq. (8), may be used to fit the data.

The GL equation was shown [25] to have a front-type solution for the rms amplitude B. This solution satisfies the following boundary conditions:

$$B(-\infty)=0\ ,\quad B(+\infty)=\sqrt{\bar{\epsilon}/g}\ ,\quad \frac{\partial B}{\partial x}(\pm\infty)=0\ .$$

The solution was obtained by a numerical integration using the Runge-Kutta method of fourth order [22]. For given $\bar{\epsilon}$ and S that were used in the experiment, the integration was carried out along a finite length $0 \le x \le L$. The initial point of the integration was at $x = L$, integrating in the direction $x = 0$ with the boundary conditions $B(L) = \sqrt{\bar{\epsilon}/g}$ and $\partial B(L)/\partial x = 0$. The integration in the opposite direction, from $x = 0$ to L, failed to produce the desired profile. This asymmetric behavior of the solution is due to the fact that the solution is stable in one direction (with $x = 0$ a fixed point in the phase space of B and $\partial B/\partial x$) and unstable in the opposite one. We found that the integration length L is a parameter that shifts the front along the x axis, and therefore tunes the healing length of the front.

Our goal was to fit the measured data points to the numerical solution of the GL equation. In order to do this, we integrated Eq. (8) for successive values of L, where L was varied at small intervals. For each value of L the ex-

perimental data points were fitted by the numerical solution with an overall multiplying factor as the fitting parameter and a least-squares fit to the solution was calculated. The solution that had the smallest variance was chosen as the appropriate one. For this solution $B(x=0)=B_0$ was obtained, and this value was taken to be the velocity amplitude associated with the noise at the inlet boundary.

[1] V. M. Zaitsev and M. I. Shliomis, Zh. Eksp. Teor. Fiz. **59**, 1583 (1970) [Sov. Phys. JETP **32**, 866 (1971)]; R. Graham, Phys. Rev. A **10**, 1762 (1974).

[2] C. W. Meyer, G. Ahlers, and D. S. Cannell, Phys. Rev. Lett. **59**, 1577 (1987); Phys. Rev. A **44**, 2514 (1991).

[3] M. Cross and P. Hohenberg, Rev. Mod. Phys. **65**, 851 (1993); H. van Beijeren and E. G. D. Cohen, J. Stat. Phys. **53**, 77 (1988).

[4] H. N. W. Lekkerkerker, Physica **80A**, 415 (1975).

[5] J. B. Swift and P. C. Hohenberg, Phys. Rev. A **15**, 319 (1977).

[6] G. Ahlers, M. C. Cross, P. C. Hohenberg, and S. Safran, J. Fluid Mech. **110**, 297 (1981).

[7] Y. Tsuchiya, K. Nakamura, and T. Kawakubo, J. Phys. Soc. Jpn. **50**, 2149 (1981).

[8] M. Sano and Y. Sawada, Phys. Rev. A **25**, 990 (1982).

[9] I. Rehberg, S. Rasenat, M. de la Torre Juarez, W. Schöpf, F. Horner, G. Ahlers, and H. R. Brand, Phys. Rev. Lett. **67**, 596 (1991).

[10] I. Rehberg, F. Hörner, L. Chiran, H. Richter, and B. L. Winkler, Phys. Rev. A **44**, R7885 (1991).

[11] W. Schöpf and I. Rehbeg, Europhys. Lett. **17**, 321 (1992).

[12] A. Tsameret and V. Steinberg, Phys. Rev. Lett. **67**, 3392 (1991).

[13] K. L. Babcock, G. Ahlers, and D. S. Cannell, Phys. Rev. Lett. **67**, 3388 (1991).

[14] A. Tsameret and V. Steinberg, preceding paper, Phys. Rev. E **49**, 1291 (1994).

[15] A. Tsameret, Ph. D. thesis, Weizmann Institute of Science, Rehovot, Israel, 1993 (unpublished).

[16] K. L. Babcock, G. Ahlers, and D. S. Cannell, Physica D **61**, 40 (1992).

[17] M. Lücke and A. Recktenwald (private communication).

[18] W. Schöpf and W. Zimmermann, Phys. Rev. E **47**, 1739 (1993).

[19] P. C. Hohenberg (private communication).

[20] *CRC Handbook of Chemistry and Physics,* 65th ed. (CRC, Boca Raton, FL, 1984), Sec. D, p. 235.

[21] F. Durst, A. Melling, and J. H. Whitelaw, *Principles and Practice of Laser-Doppler Anemometry* (Academic, London, 1976).

[22] W. H. Press, B. P. Flannery, S. A. Teukolsky, and W. T. Vetterling, *Numerical Recipes in C* (Cambridge University Press, Cambridge, England, 1988).

[23] R. J. Deissler (private communication).

[24] H. W. Müller, M. Lücke, and M. Kamps, Europhys. Lett. **10**, 451 (1989); Phys. Rev. A **45**, 3714 (1992).

[25] W. v. Saarloos, Phys. Rev. A **37**, 211 (1988).